Accepted – To appear in The Astrophysical Journal.

# Parsec-Scale Images of Flat-Spectrum Radio Sources in Seyfert Galaxies

C.G. Mundell
Department of Astronomy, University of Maryland, College Park, MD, 20742, USA;

A.S. Wilson[1]
Department of Astronomy, University of Maryland, College Park, MD, 20742, USA;

J.S. Ulvestad
National Radio Astronomy Observatory, P.O. Box O, Socorro, NM, 87801,USA;

A.L. Roy[2]
National Radio Astronomy Observatory, P.O. Box O, Socorro, NM, 87801, USA



## ABSTRACT

We present high angular resolution (∼2 mas) radio continuum observations of five Seyfert galaxies with flat-spectrum radio nuclei, using the VLBA at 8.4 GHz. The goal of the project is to test whether these flat-spectrum cores represent thermal emission from the accretion disk, as inferred previously by Gallimore et al. for NGC 1068, or non-thermal, synchrotron self-absorbed emission, which is believed to be responsible for more powerful, flat-spectrum nuclear sources in radio galaxies and quasars. In four sources (T0109−383, NGC 2110, NGC 5252, Mrk 926), the nuclear source is detected but unresolved by the VLBA, indicating brightness temperatures in excess of $10^8$ K and sizes, on average, less than 1 pc. We argue that the radio emission is non-thermal and synchrotron self-absorbed in these galaxies, but Doppler boosting by relativistic outflows is not required. Synchrotron self-absorption brightness temperatures suggest intrinsic source sizes smaller than ∼0.05−0.2pc, for these four galaxies, the smallest of which corresponds to a light-crossing time of ∼60 light days or $10^4$ gravitational radii for a $10^8$ $M_\odot$ black hole. In one of these galaxies (NGC 2110), there is also

[1]Adjunct Astronomer, Space Telescope Science Institute

[2]Present Address: MPIfR, Auf dem Hügel 69, D-53121 Bonn, Germany

extended ($\sim$0.2 pc) radio emission along the same direction as the 400-pc scale jet seen with the VLA, suggesting that the extended emission comes from the base of the jet. In another galaxy (NGC 4388), the flat-spectrum nuclear source is undetected by the VLBA. We also present MERLIN and VLA observations of this galaxy and argue that the observed, flat-spectrum, nuclear radio emission represents optically thin, free-free radiation from dense thermal gas on scales $\simeq 0.4$ to a few pc. It is notable that the two Seyfert galaxies with detected thermal nuclear radio emission (NGC 1068 and NGC 4388) both have large X-ray absorbing columns, suggesting that columns in excess of $\simeq 10^{24}$ cm$^{-2}$ are needed for such disks to be detectable.

*Subject headings:* accretion disks—galaxies:active—galaxies:jets—galaxies:nuclei—galaxies:Seyfert

## 1. Introduction

It has become generally accepted that supermassive black holes (SBH) lie at the center of most, if not all, galaxies (e.g., Richstone et al., 1998; van der Marel, 1999), with some lying dormant and others being triggered into an active phase to produce active galactic nuclei (AGN) (e.g., Haehnelt & Rees, 1993; Silk & Rees, 1998). The power source for this activity is thought to be accretion of material onto the SBH, with the infalling material forming an accretion disk which, depending on detailed conditions, then regulates the fueling rate (e.g. Narayan & Yi, 1994; Kato, Fukue & Mineshige, 1998; Blandford & Begelman, 1998). The radius to which these accretion disks extend (and hence become more easily observable) is not well established, but current AGN unification schemes advocate a geometrically thick and clumpy torus (e.g. Krolik & Begelman, 1988; Krolik and Lepp, 1989; Pier & Krolik, 1992) or warped thin disk (Miyoshi et al., 1995; Greenhill et al., 1995; Herrnstein, Greenhill & Moran, 1996; Pringle, 1996; Maloney, Begelman & Pringle, 1996) which hides the nucleus when viewed edge-on. Our viewing angle with respect to the torus or disk is then responsible for the observed differences between narrow-line AGNs (e.g Seyfert 2's), in which our view of the nuclear broad-line region is obscured (edge-on view), and unobscured (pole-on view) broad-line AGNs (e.g. Seyfert 1's). Indirect evidence in support of such tori includes the discovery of broad lines in the polarized (hence scattered) light of Seyfert 2s (Antonucci & Miller, 1985; Tran, 1995), sharp-edged bi-cones of ionized gas (e.g., Wilson & Tsvetanov, 1994) photo-ionized by anisotropic nuclear UV radiation (perhaps originating from the accretion disk and further collimated by the torus), large gas column densities ($10^{23-25}$ cm$^{-2}$) to the nuclei of Seyfert 2's, inferred from photoelectric

absorption of soft X-rays (Turner et al., 1997) and strong mid-infrared emission in both Seyfert types (e.g., Antonucci, 1993; Alonso-Herrero, Ward & Kotilainen, 1996).

Recent, high-resolution studies at optical and radio wavelengths have begun to provide more direct evidence for 'nuclear' disks on size-scales ranging from the ∼100-1000-pc diameter dusty disks imaged by HST (Jaffe et al., 1993; Ford et al., 1994; Carollo et al., 1997) and millimeter interferometry (Baker & Scoville, 1998; Downes & Solomon, 1998) to pc-scale disks inferred from HI and free-free absorption studies (Mundell et al., 1995; Carilli et al., 1998; Peck & Taylor, 1998; Wilson et al., 1998; Taylor et al., 1999; Ulvestad, Wrobel & Carilli, 1999), down to the 0.25-pc warped, edge-on, Keplerian maser disk in NGC 4258, imaged by the VLBA (Miyoshi et al., 1995, Greenhill et al., 1995; Herrnstein, et al., 1996).

Theoretical work indicates that UV/X-ray radiation from the central engine can heat, ionize and evaporate the gas on the inner edge of the torus (Pier & Voit, 1995; Balsara & Krolik, 1993; Krolik & Lepp, 1989). Indeed, simple Strömgren sphere arguments suggest a radius for the ionized region of $R(\mathrm{pc}) = 1.5\ (N_\star/10^{54}\ \mathrm{s}^{-1})^{1/3}\ (n_e/10^5\ \mathrm{cm}^{-3})^{-2/3}$, where $N_\star$ is the number of nuclear ionizing photons per second and $n_e$ is the electron density. Recalling the typical density $n_e \sim 10^{5-6}$ cm$^{-3}$ of the ionized disk in NGC 1068 (see below), we expect R ∼ 0.3−1.5 pc which is comparable to the tenths of pc to ∼pc-scale resolutions achievable with the VLBA for nearby Seyferts. Recent high angular resolution VLBA radio observations of the archetypal Seyfert 2 galaxy, NGC 1068, by Gallimore et al. (1997), have shown that emission from one of the radio components ('S1') may be associated with the inner, ionized edge of the torus. This radio component has a flat or rising (towards higher frequencies) spectrum, suggesting it contains the AGN, and a brightness temperature of up to $4 \times 10^6$ K; it is elongated perpendicular to the inner radio ejecta and extends over ∼40 mas (3 pc). The radiation mechanism may be free-free thermal emission (Gallimore et al., 1997), direct synchrotron emission (Roy et al., 1998) or Thomson scattering of a nuclear flat-spectrum synchrotron self-absorbed radio core (itself not detected) by the electrons at the inner edges of the torus (Gallimore et al., 1997; Roy et al., 1998).

This discovery highlights the possibility of using the VLBA to image the pc-scale disks or tori in other Seyfert galaxies. However, flat-spectrum radio sources in AGNs often represent non-thermal synchrotron self-absorbed radio emission with a much higher brightness temperature (>$10^8$ K) than is characteristic of component S1 in NGC 1068. High resolution radio observations are thus required to distinguish between the two emission processes. In the present paper, we report parsec-scale VLBA imaging of five Seyfert galaxies with flat-spectrum radio cores and hundred-pc scale, steep-spectrum, radio jets and lobes. Two of these galaxies also exhibit ionization cones with sharp, straight edges and axes aligned with the radio ejecta. Our goal is to determine whether the flat spectrum

nuclear radio emission represents thermal emission from the accretion disk/obscuring torus or synchrotron self-absorbed emission from a compact radio core source.

The paper is organized as follows; Sections 2 and 3 describe the sample selection, observations and reduction techniques whilst in Section 4, the results of the study are presented. Section 5 discusses possible scenarios for the observed radio emission including direct non-thermal radiation from the AGN, emission from supernovae or supernova remnants produced in a starburst, or thermal emission from the accretion disk. The observed brightness temperatures are discussed in the context of the NGC 1068 result and comparison is made with other types of active nuclei such as radio galaxies, radio-loud and radio-quiet quasars. Section 6 summarizes the conclusions. Throughout, we assume $H_0 = 75$ km s$^{-1}$ Mpc$^{-1}$ and $q_0 = 0.5$.

## 2. Sample Selection

The radio emission of Seyfert galaxies imaged at resolutions $0\farcs1$–$1''$ almost always has the steep spectrum characteristic of optically thin synchrotron radiation. Flat spectrum cores are rare. In order to identify galaxies that may contain radio components similar to 'S1' in NGC 1068, we have reviewed both published (e.g., Ulvestad & Wilson, 1989, and earlier papers in this series at $\lambda$6 cm and $\lambda$20 cm; Kukula et al., 1995 at 3.6 cm) and unpublished (Wilson, Braatz & Dressel at 3.6 cm) VLA 'A' configuration surveys and other interferometric studies (e.g., Roy et al., 1994). In selecting candidate galaxies for VLBA observations, we used the following criteria:

• The radio component that is coincident with the optical nucleus (the position of which is known to $\approx 0\farcs2$ accuracy – e.g., Clements, 1981, 1983), has a flat spectrum ($\alpha \leq 0.4$, $S \propto \nu^{-\alpha}$) between 20 cm and 6 cm or 3.6 cm with the VLA in 'A' configuration. This component must also be unresolved in the VLA 'A' configuration at 2cm and/or 3.6 cm.

• The flux density of this component exceeds 5 mJy at 3.6 cm (for comparison, the total flux density of component 'S1' in NGC 1068 at this wavelength is 14 mJy).

• There is, in addition, extended, 'linear' (double, triple or jet-like), steep spectrum radio emission on the hundreds of parsecs – kiloparsec scales, or well-defined, optical ionization cones. The reason for this last criterion is to define the axis of ejection of the radio components and thus the expected axis of the accretion disk.

We found only six (excluding NGC 1068) Seyfert galaxies that satisfy these three criteria in the entire sample of about 130 imaged in the 'A' configuration. We omit one of

them because of its unfavorable declination (–44°), leaving five for imaging with the VLBA. These galaxies are T0109−383, NGC 2110, NGC 4388, NGC 5252 and Mrk 926.

## 3. Observations and Reduction

### 3.1. VLBA Observations

The observations were obtained with the 10-element VLBA (Napier et al, 1994) at 8.4 GHz during observing runs in 1997 and 1998, details of which are given in Table 1. Dual circular polarizations (Right & Left) were recorded for all sources, and only the parallel hands (i.e. RR and LL) were correlated. T0109−383, NGC 2110 and Mrk 926 were recorded with a 32-MHz bandwidth and two-bit sampling (8 MHz per IF, 4 IFs, 2 polarizations) and NGC 4388 and NGC 5252 were recorded with a 16-MHz bandwidth and two-bit sampling.

The target sources are too weak to obtain estimates of the phase errors using standard VLBI self-calibration/imaging techniques (e.g. Walker, 1995); instead the targets were observed in phase referencing mode, in which frequent observations of a nearby bright calibrator are interleaved with target scans and used for fringe fitting, which corrects the large phase errors, delays (phase variations as a function of frequency) and delay rates (phase variations as a function of time) present in the data (Beasley & Conway, 1995). As described below, extending the coherence time in this way improves the signal-to-noise ratio and enables an image of the target source to be made, which can then be used as a starting model for subsequent cycles of self-calibration. Target source plus phase calibrator cycle times are shown in Table 1. This method is similar to that used on smaller, connected-element arrays, such as the VLA (known as 'phase calibration'), but is more problematic for VLBI due to larger and more rapidly varying phase errors. Rapid changes in the troposphere at 8.4 GHz therefore require short switching times to satisfy the condition that the change in atmospheric phase be less than a radian over the switching interval, thus enabling reliable phase connection, without $2\pi$-radian ambiguities, for successful imaging of the target source (Beasley & Conway, 1995). In addition, less frequent observations were made of a bright calibrator ('phase check') source.

Data editing and calibration followed standard methods (Greisen & Murphy, 1998) and used the NRAO Astronomical Image Processing System (AIPS) (van Moorsel, Kemball & Greisen, 1996). Amplitude scales were determined from standard VLBA antenna gain tables, maintained by NRAO staff, and measurements of $T_{\rm sys}$ made throughout the run. In addition, all data for source elevations below $\sim$5° were removed, and the antennas at Hancock (HN), and North Liberty (NL) were deleted from the NGC 5252 dataset as no

fringes were detected to HN, and NL showed poor phase stability due to bad weather. The final phase corrections, interpolated over time, were used as a guide for additional data editing.

Despite short switching times between galaxy and phase calibrator, poor tropospheric conditions and uncertainty in the target source position prevented immediate imaging of the phase-referenced target sources using all the data. Observations of the 'phase check' source were therefore used to verify the quality of the phase referencing, before applying the phase corrections to the target sources, and to provide ancillary calibration such as manual pulse calibration and amplitude calibration checks.

After imaging the phase calibrator to verify that the corrections derived from fringe fitting were valid, phase, delay and rate corrections were applied to the 'check source', from phase calibrator scans that were adjacent in time to the check source. Many baselines displayed poor phase coherence at some point in the observing run, preventing a coherent image of the source from being produced initially from the whole dataset. Instead, small time ranges (e.g. around 1 hour), within which the majority of antennas had less rapidly varying phases, were selected to be used in the initial stages of the imaging process. The 'check' source, with calibration applied from the phase calibrator, was imaged for the selected small time range. The resultant image was then used as an input/starting model for subsequent cycles of self-calibration. This self-calibration process then enabled the remaining data to be fully calibrated and used to make a final image of the 'check' source. The final structure, flux and position of each 'check' source compared well with previously published images (e.g. Browne et al., 1998; Fey & Charlot, 1997) and images produced from our data using self-calibration alone. This method provides an independent consistency check on the phase referencing, increasing our confidence in the images of the target sources. Only one 'check' source (J0044-3530) was not successfully imaged due to insufficient data (i.e. only 3 minutes at very low elevation). The target sources were then imaged using the same method, with natural and uniform data weighting. The uniformly weighted images (with robust parameter 0 - Briggs, 1995) are shown in Figure 1. The naturally weighted images, with more sensitivity to extended emission, were used to derive the brightness temperature limits to possible thermal emission from the program galaxies; these limits are $\sim$30% lower than those derived from the uniformly weighted images shown in this paper.

The uncertainty in the flux scale is taken to be $\sim$5% and is included in the total uncertainties in flux densities quoted in Table 2. These errors were derived by adding, in quadrature, the 5% amplitude scale error, the r.m.s. noise in the final image and the error in the Gaussian fitting.

The accuracy of the target source positions is dominated by the uncertainty in the

position of the phase calibrators (∼0.4 – 14 mas; see Table 1). Additional positional errors, due to the transfer of phase corrections from the phase calibrator to the target source, are negligible due to the promixity of each calibrator to its target source.

### 3.2. MERLIN observations

NGC 4388 was not detected by the present VLBA observations. We therefore obtained and analyzed MERLIN $\lambda$6-cm (4.993-GHz) archival data for NGC 4388, which was observed on 7th December, 1992 with six antennas. Phase referencing was performed with regular observations of 1215+113, interleaved throughout the observing run and 3C286 was used for flux and bandpass calibration. A flux of 7.087 Jy for 3C286 was adopted, assuming a total flux density of 7.382 Jy (Baars et al., 1977) and correcting for MERLIN resolution effects. After initial gain-elevation corrections and amplitude calibration using MERLIN software, the data were transferred to AIPS for all subsequent phase and amplitude calibration, data editing and imaging. Dual polarizations were recorded for a 15-MHz bandwidth, centered at 4.993 GHz, but the right circular polarization data were removed due to instrumental problems, resulting in a final image of the left circular polarization only (Figure 2).

## 4. Results

Five flat-spectrum-core Seyferts, were observed with the VLBA at 8.4 GHz. Four of the five sources were detected (T0109−383, NGC 2110, NGC 5252, Mrk 926) and show compact, unresolved cores with brightness temperatures $T_B > 10^8$ K, total luminosities at 8.4 GHz of $\sim 10^{21}$ W Hz$^{-1}$ and sizes, on average, less than 1 pc. In addition to the core emission, NGC 2110 shows extended emission which may represent the inner parts of the radio jets, and NGC 5252 may be marginally extended (Figure 1). NGC 4388 is not detected with the VLBA, but is detected at 5 GHz with MERLIN (Figure 2). We find no evidence for emission (to a 3-$\sigma$ limit of $T_B \sim 10^6$ K) extended perpendicular to the hundred-pc scale radio emission in T0109−383, NGC 2110, NGC 5252 or Mrk 926, as would be expected for emission from an accretion disk, but we discuss the possibility of thermal emission from NGC 4388 (Section 5.4). The measured and derived properties of each source are listed in Table 2, while more detailed properties of NGC 2110 and NGC 4388 are given in Tables 3 and 4 respectively. The properties of each source are discussed more fully below. Distances are calculated assuming $H_0 = 75$ km s$^{-1}$ Mpc$^{-1}$ and $q_0 = 0.5$, except for NGC 4388 which is assumed to be at the distance of the Virgo cluster, taken to be 16 Mpc.

### 4.1. T0109−383

T0109−383 (NGC 424) is a highly inclined (∼75°) early-type ((R)SB(r)0/a – de Vaucouleurs et al. 1991) Seyfert galaxy at a distance of 46.6 Mpc. The nucleus of T0109−383, originally classified as a Seyfert type 2 (Smith, 1975), exhibits strong line emission from highly ionized species such as [Fe VII]$\lambda$5720,6086 and [Fe X]$\lambda$6374 (Fosbury & Sansom, 1983; Penston et al., 1984). Analysis of the continuum emission from the far IR to the far UV and decomposition of the H$\alpha$ – [NII] blend led Boisson & Durret (1986) to suggest a re-classification of T0109−383 to a Seyfert 1. The recent discovery of broad components to the H$\alpha$ and H$\beta$ lines, along with emission from Fe II, confirms the type 1 classification (Murayama et al., 1998). VLA images of the radio emission at 6 and 20 cm, show the nuclear radio source to consist of an unresolved core with a flat spectrum ($\alpha_6^{20}$=0.17±0.07) between $\lambda$6 and $\lambda$20 cm, and a weaker, secondary, steep spectrum component $\simeq$1.″4 east of the core (Ulvestad & Wilson, 1989). Similar radio structure is seen in the 8.4-GHz VLA image (Braatz, Wilson & Dressel, unpublished), shown in Figure 1, with the core spectrum remaining relatively flat ($\alpha_{3.5}^{6}$=0.21) between 6 and 3.5 cm (Morganti et al., 1999). The results of Gaussian fitting to the 8.4-GHz VLBA image (Figure 1), given in Table 2, show the sub-pc scale nuclear emission to be unresolved, with a peak brightness of $T_B > 8.1 \times 10^8$ K, adopting a source size smaller than half of the beamsize. The peak and integrated 8.4-GHz VLA fluxes for the core, 10.4 mJy beam$^{-1}$ and 11.2 mJy respectively, are in excellent agreement with those measured from the VLBA image (Table 2), indicating that little nuclear emission was missed by the VLBA. A similar peak brightness of 10.4 mJy beam$^{-1}$ is found in the 3.5-cm ATCA image of Morganti et al. (1999), while their slightly higher integrated flux includes some of the emission $\simeq 1''$ E and W of the nucleus (Ulvestad & Wilson, 1989; Figure 1). The excellent agreement between the nuclear $\lambda$3.6-cm fluxes in observations spanning ∼six years indicates no significant variability.

In the VLBA image, we detected no extended emission in the N-S direction (as might be expected from a parsec-scale, thermal disk if the arcsec-scale, steep spectrum, E-W emission in the VLA image is interpreted as emission from nuclear ejecta) brighter than $\sim 1.3 \times 10^6$ K ($3\sigma$ in the naturally weighted image) and more extended than 0.27 pc (half of the beamsize in the naturally weighted image).

### 4.2. NGC 2110

NGC 2110 was initially classified as a Narrow Line X-ray Galaxy, NLXG, (Bradt et al., 1978), and lies in an S0/E host galaxy (Wilson, Baldwin & Ulvestad, 1985) at a distance

of 30.4 Mpc. Such NLXG's have a sufficient column of dust to the nucleus to obscure the broad line region, thus leading to a Seyfert 2 classification of the optical spectrum, but an insufficient gas column to attenuate the 2–10 keV emission, so the hard X-ray luminosity is comparable to those of Seyfert 1's (Weaver et al., 1995a; Malaguti et al., 1999). Early radio observations found NGC 2110 to be a strong radio source (Bradt et al., 1978) and subsequent VLA imaging (Ulvestad & Wilson, 1983; 1984b) showed symmetrical, jet-like radio emission, extending $\sim$4″ in the N-S direction and straddling a central compact core. A more recent VLA A-configuration image at $\lambda$3.6 cm, obtained by Nagar et al. (1999) and shown in Figure 1, contains a wealth of complex structure. Ulvestad & Wilson (1983) found the spectrum of the core to be relatively flat (spectral index $\alpha_6^{20}$ $\sim$0.36$\pm$0.05) between $\lambda$20 cm and $\lambda$6 cm, but becoming steeper ($\alpha_2^6\sim$0.96$\pm$0.09) between $\lambda$6 cm and $\lambda$2 cm (assuming no time variability). Using the $\lambda$3.6-cm core flux measurement of Nagar et al. (1999) and ignoring variability or resolution effects gives spectral indices of $\alpha_{3.6}^6 = 0.61$ and $\alpha_2^{3.6} = 1.31$, also suggesting a steepening of the spectrum at higher frequencies.

The radio continuum emission of NGC 2110, imaged with the VLBA at $\lambda$3.6 cm and shown in Figure 1, consists of a compact core, presumably the nucleus, and slightly extended emission which is most pronounced to the north. The results of fitting a single-component Gaussian are given in Table 2; the fact that the integrated flux is significantly higher than the peak flux also suggests the source is resolved. Resolved structure is also evident in the time-averaged $(u, v)$ data (not shown), consistent with an unresolved point source (with a flux density of $\sim$ 8 mJy) superimposed on an extended "halo" with approximate dimensions of 2.5 (N-S) $\times$ 0.5 (E-W) mas. Preliminary two-component Gaussian fits to the image are also consistent with an unresolved point source and an extended component. We therefore subtracted an 8-mJy point source (in the $(u, v)$ plane using the AIPS task UVSUB) positioned at the peak of the 3.6 cm VLBA image, and studied the residual emission. This emission is extended both north and south of the core by $\sim$0.7 mas, consistent with emission from the inner regions of the northern and southern jets.

Using the brightness of 8 mJy beam$^{-1}$ for the unresolved component and assuming an upper limit to the source size of 0.94 $\times$ 0.36 mas (half of the beamsize), we find $T_B > 6.0 \times 10^8$ K. In addition to the core and extended emission, the Gaussian fits suggest the presence of a third component, centered $\sim$1.95 mas north of the core; its size and direction of elongation are not well constrained. This component may be a knot in the northern jet. A summary of the fitted properties of each component is given in Table 3.

The total VLBA-detected flux density of the source (zero baseline flux measured in the UV plane) is 30 mJy. This flux density is lower than the previously measured VLA core flux of 77.6 mJy at this frequency (Nagar et al., 1999), presumably due to the high spatial

resolution of the present observations and missing short spacings of the VLBA compared to the VLA, thereby reducing our sensitivity to extended structure. This may also explain why we detect no VLBA counterpart to the small eastern extension present in the $\lambda$3.6-cm VLA image, which contains about 3.6 mJy of flux and extends approximately $0\farcs5$ east of the core (Nagar et al., 1999). Alternatively, the extension in the VLA image may be a result of instrumental effects caused by the source position being close to the celestial equator and the short duration of the snapshot observation, an effect termed 'equator disease' (Antonucci & Ulvestad, 1985). In the VLBA image, we detect no extended emission in the E-W direction (such as might be expected from a parsec-scale thermal disk) brighter than $3.1 \times 10^6$ K ($3\sigma$ in the naturally weighted image), and more extended than 0.07 pc (one half of the E-W beamsize in the naturally weighted image).

### 4.3. NGC 4388

NGC 4388 is a nearby, edge-on spiral galaxy (SB(s)b pec - Phillips & Malin, 1982) which is thought to lie close to the centre of the Virgo cluster (Phillips & Malin, 1982) and may be tidally disturbed by nearby cluster core galaxies M84 or IC3303 (Corbin, Baldwin & Wilson, 1988). Ionization cones extend approximately perpendicular to the disk (Pogge, 1988; Corbin et al., 1988; Falcke, Wilson & Simpson, 1998) and the kinematics of the ionized gas in the narrow line region (NLR) shows a complex combination of rotation and outflow (Corbin et al. 1988; Veilleux, 1991; Veilleux et al., 1999). The nucleus is variously classified as Seyfert type 1 or 2, with the high galactic inclination and obscuring dust lanes making unambiguous classification difficult (Falcke et al., 1998). Shields & Filippenko (1988) report broad, off-nuclear H$\alpha$ emission, but subsequent IR searches for broad lines such as Pa$\beta$ (Blanco, Ward & Wright, 1990; Ruiz, Rieke & Schmidt, 1994) and Br$\alpha$ and Br$\gamma$ (Veilleux, Goodrich & Hill, 1997) have failed to detect a broad nuclear component.

Previous radio continuum images of NGC 4388 (Stone et al., 1988; Carral, Turner & Ho, 1990; Hummel & Saikia, 1991; Falcke et al., 1998) show complex, extended structure, both along the galactic plane and perpendicular to it. A recent 3.5 cm VLA image of the extended radio emission (Falcke et al., 1998) shows, in more detail, the 'hour-glass'-shaped radio outflow to the north of the galactic plane, and the compact ($\sim 1\farcs9$ separation) central double, which were suggested by earlier images. In Section 4.3.1 we concentrate on the radio emission from the northern component of the compact radio double, which shows a flat spectrum up to 2 cm (Carral, Turner & Ho, 1990) and is thought to be the nucleus, and in Section 4.3.2, we discuss the extended emission to the SW.

### *4.3.1. The nucleus*

As stated earlier, NGC 4388 is not detected in the 8.4-GHz VLBA observations, with a 3-$\sigma$ brightness temperature limit of $T_B \lesssim 2.2 \times 10^6$ K ($\sigma$=63.2 $\mu$Jy/beam with a beam size of 2.52 × 1.46 mas in the naturally weighted map, with a factor 1.7 applied to correct for decorrelation due to residual imperfections in the phase referencing corrections, estimated using the check source). We do, however, detect emission from NGC 4388 at $\lambda$6cm with MERLIN. The uniformly weighted MERLIN image (Figure 2) shows emission from two components, labelled M1 and M2, the stronger of which we identify with the nucleus and discuss in more detail here, while M2 is discussed in Section 4.3.2. The nuclear component M1, has a peak brightness of 1.2 mJy beam$^{-1}$ which corresponds to a brightness temperature $T_B > 2.4 \times 10^4$ K at 5 GHz (beamsize 91 × 39.5 mas, see Table 4). The nucleus is unresolved in the MERLIN data, indicating that the source size is intermediate between the MERLIN and VLBA beam sizes. However, a combination of the MERLIN and VLBA results with published spectral index information can further constrain the source size.

Earlier radio observations of NGC 4388 have found the nuclear spectrum to be flat from 1.49 GHz to 15 GHz. The spectral index was measured to be $\alpha = 0.26$ between 1.49 GHz and 4.86 GHz with a relatively large beamsize of 1$''$.2 (Hummel & Saikia, 1991) and Carral et al. (1990) report a flat spectrum up to 15 GHz with an upper limit to the nuclear size of 70 mas. Including the VLA 8.4 GHz core flux of Kukula et al (1995) suggests that the spectrum of the nucleus may be very slightly inverted between 8.4 GHz and 15 GHz ($\alpha = -0.05$) but within the errors it can be taken as flat. We therefore used the measured MERLIN 5-GHz peak flux to derive *predicted* VLBA 8.4 GHz fluxes of the nucleus, for spectral indices of both $\alpha = 0.0$ and 0.26, and converted these predicted fluxes to brightness temperatures, assuming the source is unresolved by the representative VLBA beamsize of 2.52 × 1.46 mas.

These predicted temperatures are listed in Table 4 and are above the detection threshold of the VLBA observations for a source size equal to or smaller than the VLBA beam. The larger predicted brightness temperature, for a source size equal to the VLBA beam, of $T_B \simeq 8.3 \times 10^6$ K is, however, only 3.8 times greater than our 3-$\sigma$, VLBA detection limit and so the solid angle of the source need only be 3.8 times larger than the VLBA beamsize to be undetected. We therefore constrain the size of the nucleus to be $\gtrsim$ 3.7 mas ($\alpha$=0.0) or $\gtrsim$ 0.3 pc. Sensitive, high angular resolution VLBA observations at lower frequencies such as 2.3 GHz and 1.4 GHz are required to determine the actual size and structure of the nucleus in NGC 4388.

#### *4.3.2. Collimated radio emission*

In addition to the core emission at 5 GHz, the MERLIN image of NGC 4388 shows a second weak component SW of the nucleus (labelled M2 in Figure 2). This component is only $\sim$0.25″ away from the nucleus, lying along PA $\sim$211° with respect to the core, and should not be confused with the stronger, more distant radio component seen in previous VLA images (e.g. Falcke et al, 1998), which lies $\sim$1.″9 from the nucleus (in PA $\sim$201°). To establish the reality of this weak MERLIN component, the VLA 8.4-GHz data (published by Falcke et al., 1998) were re-examined. The uniformly weighted image, shown in Figure 3a, has a rather elongated synthesized beam of size 0.″7 × 0.″22 (PA 74°), but a bridge of emission is clearly visible, connecting the two main radio components (labelled V1 & V2). A similar bridge of emission was seen in the 4.86-GHz VLA image of Hummel & Saikia (1991) and the 8.4-GHz VLA snapshot image of Kukula et al. (1995). The crosses indicate the positions of the nucleus and the weak component (M2) visible in the MERLIN 5 GHz image. Figure 3b shows a super-resolved image produced from the same VLA data, with a circular synthesized beam of 0.″22. Again the crosses mark the MERLIN components, and an extension of the 8.4 GHz VLA emission is seen at the location of the weak MERLIN component M2, further suggesting that the MERLIN emission is real. The super-resolved image also suggests that a well-collimated jet of emission is emanating from the core (V1) along PA $\sim$210° for $\sim$1.″5, before changing direction at V2. The MERLIN component M2 would then be an inner part of this collimated radio ejection. Falcke et al (1998) find a good association between V2 and a 'spike' of optical line emission, suggesting interaction of the radio jet with a cloud in the NLR. The 'hooked' shape of the southern radio jet, suggested by Fig. 3b, is reminiscent of similarly well-collimated radio jets seen in an increasing number of Seyferts (e.g., Mrk 34 - Falcke et al., 1998; Mrk 3 - Kukula et al. 1993; NGC 1068 - Wilson & Ulvestad, 1983; NGC 2110 - Ulvestad & Wilson, 1983; Nagar et al., 1999), which are deflected or terminate at radio hot spots. However, sensitive high angular resolution radio observations are required to image the detailed structure of the proposed radio jet in NGC 4388.

### 4.4. NGC 5252

NGC 5252, an S0 galaxy (de Vaucouleurs et al., 1991) with a Seyfert type 1.9 nucleus (Acosta-Pulido et al., 1996), exhibits a dramatic bi-cone of ionized gas (Tadhunter & Tsvetanov, 1989; Wilson & Tsvetanov, 1994; Acosta-Pulido et al., 1996) extending $\sim$35 kpc from the nucleus (along PA 165°) and argued to be ionized by anisotropic nuclear UV radiation. The intrinsic anisotropy of the ionizing radiation was nicely confirmed by HI

$\lambda$21-cm images, which show neutral hydrogen filling the regions outside the bi-cone (Prieto & Freudling, 1993, 1996).

Observations with the VLA (Wilson & Tsvetanov, 1994) show a radio structure consisting of a central, compact core, with a relatively flat spectrum between $\lambda$20 cm and $\lambda$6 cm ($\alpha_6^{20} = 0.22$), steepening at shorter wavelengths ($\alpha_{3.6}^{6} = 0.78$), and weaker emission extending $\sim$2″ north (PA $\sim$345°) and south (PA $\sim$175°) of the core. A second compact radio component, seen $\sim$22″ north (PA –8.°9) of the nucleus, may be associated with NGC 5252, lying close to the PA of the extended core emission and coinciding with a region of high excitation ionized gas (Wilson & Tsvetanov, 1994), or may be a background source (Morse et al., 1998). More recent radio images by Nagar et al. (1999) at $\lambda$20 cm and $\lambda$3.6 cm confirm the overall spectrum of the core ($\alpha_{3.6}^{20} = 0.32$) and the radio continuum features seen in the earlier images.

The 8.4-GHz VLBA image of the core of NGC 5252 is shown in Figure 1, along with the larger scale $\lambda$20-cm VLA image (from Nagar et al., 1999), and the results of Gaussian fitting to the emission are detailed in Table 2. The deconvolved size of the core is less than half of the beamsize and so we classify the emission as unresolved. The peak brightness of 7.9 mJy beam$^{-1}$ (corresponding to $T_B > 4.2 \times 10^8$ K) is in agreement with that measured by Nagar et al. (1999) – 7.9 mJy beam$^{-1}$ – and slightly higher than that found by Wilson & Tsvetanov (1994) – 6.7 mJy beam$^{-1}$. The integrated VLBA flux (9.1 mJy) is also very similar to that of Nagar et al. (1999) (9.3 mJy). The similarity of the VLBA- and VLA-measured nuclear fluxes indicates that little emission was missed by the VLBA. The fact that the measured integrated VLBA flux is $\sim$15% higher than the peak and the possible visible extension to the SW (Fig. 1) are evidence for weak extended emission. The quality of the data, however, make this detection tentative and higher sensitivity observations are required to confirm the extension and determine its structure.

### 4.5. Mrk 926

Mrk 926 (MCG-2-58-22), the most distant object in our sample at $z$=0.0473, is a type 1 Seyfert and was first identified as a Seyfert through its luminous ($L_x = 5 \times 10^{44}$ erg s$^{-1}$) X-ray emission (Ward et al. 1978). Later X-ray observations found a relatively flat X-ray spectrum (although detailed model fits are controversial - George et al., 1998) and Weaver et al. (1995b) suggested that their ASCA observations of Mrk 926 were consistent with a "bare" Seyfert 1 nucleus. X ray variability, with a 14 year timescale, provides an upper limit of 4.3 pc for the size of the emitting region (Weaver et al., 1995b).

The 8.4 GHz VLA image (Braatz, Wilson & Dressel, unpublished), shown in Figure 1, shows a compact core with weak E-W extensions confirming the earlier 6-cm image (Ulvestad & Wilson, 1984a). The nuclear radio spectrum is relatively flat between $\lambda$6 cm and $\lambda$3.6 ($\alpha^{6}_{3.6} = 0.24$), but steepens at longer wavelengths ($\alpha^{20}_{6} = 1.1$). This steepening of the spectrum may, in part, be due to inclusion of the extended E-W emission in the low resolution $\lambda$20-cm observation (Wilson & Meurs, 1982), but is also consistent with a lack of free-free absorption toward the nucleus, supporting the X-ray classification as a "bare" Seyfert 1 nucleus. The 8.4-GHz VLBA image (Figure 1) shows an unresolved source. The results of Gaussian fitting to the VLBA detection of Mrk 926 and corresponding derived quantities are given in Table 2. A peak brightness of 7.5 mJy beam $^{-1}$ is measured in the VLA image while the peak brightness in the VLBA image is 4.6 mJy beam$^{-1}$. No additional extended flux is present in the VLBA data as can be seen from the image (to a 3-$\sigma$ limit of $T_B < 1.3 \times 10^6$ K) and the agreement between the peak and integrated flux densities (Table 2). The upper limit to the size of the unresolved core is $\sim$1.3 $\times$ 0.5 pc (half of the beamsize). The fact that less flux is detected with the VLBA than the VLA, however, suggests additional emission, extended on scales between the VLA ($0\farcs27 \times 0\farcs21$) and VLBA beams (2.8 $\times$ 1.0 mas), or time variability.

## 5. Discussion

### 5.1. Compact Cores and Flat Spectra

In contrast to the commonly observed high brightness temperature, flat spectrum cores in quasars, blazars and radio galaxies (e.g. Pearson et al., 1998; Kellerman et al., 1998, Hough et al., 1999), flat spectrum cores in Seyfert galaxies appear to be rare (e.g. de Bruyn & Wilson 1978; Sadler et al., 1995; Morganti et al., 1999), with only $\sim$10% detected in the sample of de Bruyn and Wilson (1978). High brightness temperature, flat spectrum cores are thought to represent the synchrotron self-absorbed base of a relativistic jet produced by the central engine (e.g., Peterson, 1997), while the steep spectrum components are considered to be associated with shocks along the jet. Despite the small linear extents of Seyfert radio jets compared with those in quasars and radio galaxies, the relative proximity of Seyferts permits higher linear resolution to be achieved at comparable angular resolutions to studies of quasars and radio galaxies. However, various factors, such as free-free absorption by broad line region (BLR) or other dense gas and dominance by steep spectrum emission, may make it difficult to detect flat spectrum radio cores in Seyfert galaxies. In addition, evidence is mounting that Seyfert radio jets are not relativistic (Ulvestad et al., 1999), but instead may be thermally dominated (Bicknell et al., 1998; Wilson & Raymond,

1999), thereby removing Doppler boosting of the putative flat spectrum core emission as a means for increasing its detectability.

As shown by recent studies of NGC 1068 (Gallimore et al., 1997; Roy et al., 1998) an alternative explanation for flat spectrum cores in Seyferts is emission from the obscuring torus itself, either as thermal bremsstrahlung (Gallimore et al., 1997), direct synchrotron radiation (Roy et al., 1998) or scattered synchrotron radiation from a self-absorbed core (Gallimore et al., 1997; Roy et al., 1998). Here, we discuss our results in this context, examining whether the emission is likely to be thermal or non-thermal, central engine or starburst related and whether, if associated with a central engine, Doppler boosting could be important.

### 5.2. Nuclear emission - thermal or non-thermal?

High angular resolution 8.4-GHz VLBA observations of the flat-spectrum nuclear component, 'S1', in NGC 1068 have revealed an edge-on, disk-like structure, aligned roughly perpendicular to the radio jet axis, with an extent of $\sim$0.5 pc and a brightness temperature ranging from $\sim 5 \times 10^5$ to $3.7 \times 10^6$ K (Gallimore et al., 1997). In contrast, we find high $T_B$ ($>10^8$ K), unresolved ($<$1 pc) cores in T0109−383, NGC 2110, NGC 5252 and Mrk 926, consistent with non-thermal emission. The brightness temperature of a synchrotron self-absorbed source is $T_B \simeq \gamma m_e c^2/3k \simeq 2.0 \times 10^9 \gamma$ K, where $\gamma$ is the Lorentz factor, $m_e$ the electron mass, c the speed of light and k Boltzmann's constant. The maximum $T_B$ for such a source is $\sim 10^{12}$ K, limited by the "inverse Compton catastrophe", in which cooling by inverse Compton scattering quickly reduces the brightness temperature to $10^{11-12}$ K (e.g., Kellermann & Pauliny-Toth, 1969; Kellermann & Pauliny-Toth, 1981). Readhead et al. (1994) argue that a more physical limit is the equipartition brightness temperature, which limits the intrinsic brightness temperature in the emission rest frame to be $\sim 10^{11}$ K (consistent with average observed values - Lähteenmäki, Valtaoja & Wiik, 1999). Although observed $T_B$'s as high as $10^{16}$ K have been inferred from intra-day variability seen in some blazars (e.g., Crusius-Waetzel & Lesch, 1998), and in one extreme case, intra-hour variability in the quasar PKS 0405−385, suggesting $T_B \sim 10^{21}$ K if the variability is intrinsic to the source or $T_B > 5 \times 10^{14}$ K if explained by interstellar scintillation of a source smaller than 5$\mu$as (Kedziora-Chudczer et al., 1997), the brightness of these objects is thought to be extremely Doppler boosted by relativistic outflows. Our measured lower limits to the $T_B$ of T0109−383, NGC 2110, NGC 5252 and Mrk 926 are in the range $(2-8) \times 10^8$ K and are therefore consistent with synchrotron self-absorption, but do not require Doppler boosting. For $\gamma$=1, the intrinsic brightness temperature of a self-absorbed

source is $2 \times 10^9$ K, suggesting source sizes smaller than $\sim$0.2$-$0.3 mas, or $\sim$0.05$-$0.2pc, for these four galaxies, the smallest of which corresponds to a light-crossing time of $\sim$60 light days or $10^4$ gravitational radii for a $10^8$ $M_\odot$ black hole. Such small sources may be resolved at 8 GHz with future space VLBI missions such as ARISE (Ulvestad, Gurvits & Linfield, 1997; Ulvestad & Linfield, 1998).

The spectra of the nuclei of NGC 5252 and NGC 2110 appear to steepen towards higher frequencies (as discussed in Section 4), consistent with the cores becoming optically thin to synchrotron self-absorption at $\sim\lambda$6 cm (as suggested for NGC 5252 by Wilson & Tsvetanov, 1994). Alternatively, free-free absorption by ionized gas, with optical depths $\tau_{\rm ff}(1.4\ {\rm GHz}) \lesssim 0.6$, could account for the observed spectral indices between $\lambda$20 cm and $\lambda$6 cm for T0109, NGC2110 and NGC5252, assuming that the intrinsic emission is optically thin synchrotron with $\alpha_6^{20} = 0.7$.

No evidence of thermal disk-like emission, extended perpendicular to the collimation axis, is found in these sources to a 3-$\sigma$ limit of $\sim 10^6$ K (see Figure 1). Any emission similar to the brighter, inner (0.5-pc) disk in NGC 1068, could just be spatially resolved in T0109$-$383, NGC 2110 and NGC 5252, but not in more distant objects like Mrk 926. Nevertheless, these four Seyferts are dominated by the compact, high $T_B$ core emission which is completely different from NGC 1068, which shows no compact, unresolved core. The absence of a bright core in NGC 1068 may reflect absorption by a BLR cloud or by the (probably) thermal disk seen in radio continuum. As we discuss below, a high column density of ionized gas in such a disk is needed for detectable thermal radio emission and the disk could hide the compact, high brightness core through free-free absorption. The column density towards the nucleus of NGC 1068 is thought to be so high ($>10^{26}$ cm$^{-2}$ – Matt et al., 1997) that it is optically thick to Compton scattering and the nucleus is totally hidden from view even in hard X-rays. The X-ray inferred column densities for three of the core-dominated Seyferts are significantly lower at $2.4 \times 10^{22}$ cm$^{-2}$ for NGC 2110 (Weaver et al., 1995a), $3.4 \times 10^{22}$ cm$^{-2}$ for NGC 5252 (Turner et al., 1997) and $\sim 5.7 \times 10^{20}$ cm$^{-2}$ for Mrk 926 (Weaver et al., 1995b).

Given the detection of the sub-pc scale, non-thermal radio sources, the disk cannot be optically thick to free-free absorption if the synchrotron self-absorbed radio core is seen through it. We may then calculate an upper limit to the thermal radio emission from the disk by assuming $\tau_{\rm ff}(8.4\ {\rm GHz}) \lesssim 0.5$ and that the entire column density inferred from X-ray photoelectric absorption is fully ionized. As the disks in NGC 2110 and NGC 5252 are expected to lie along the beam minor axis, we assume a conservative upper limit to the disk diameter of twice the minor axis beamsize and use the height to diameter ratio of 2:1 as found for NGC 1068, giving maximum disk dimensions of $0.22 \times 0.11$ pc and $0.86 \times 0.43$ pc

for NGC 2110 and NGC 5252 respectively[3]. The assumed upper limits to the disk size, column density and free-free optical depth yield lower limits to both the electron densities $n_e \sim 7.3 \times 10^4$ cm$^{-3}$ and $2.6 \times 10^4$ cm$^{-3}$, and electron temperatures $T_e \sim 3 \times 10^4$ K and $1.8 \times 10^4$ K for NGC 2110 and NGC 5252 respectively, and therefore a maximum predicted 8.4-GHz flux of 1.4 $\mu$Jy for both, undetectable with present observations. These calculations indicate that thermal radio emission from an accretion disk is most likely to be detected from nuclei with high ($>10^{24}$ cm$^{-2}$) X-ray inferred column densities, as may be the case for NGC 4388 (see Section 5.4). Thus, further insight into the nature of thermal radio cores in Seyferts might be gained with milliarcsecond-resolution observations of galaxies with high ($>10^{24}$ cm$^{-2}$) X-ray inferred column densities.

### 5.3. Seyfert nuclei - starburst or accretion-powered central engine?

A key question is whether the nuclear power source in radio-quiet quasars, Seyferts and ultra-luminous infrared galaxies is a compact starburst or accretion onto a supermassive black hole. Whilst emission from hot stars in the torus might account for the featureless continua in Seyfert 2's (Fernandes & Terlevich 1995; González-Delgado et al. 1998), it seems that starbursts cannot provide the necessary collimation to produce radio jets. The existence of radio jets is, therefore, often used as an indication of the presence of a black hole plus accretion disk. Although some Seyferts are now known to possess strikingly collimated jets (e.g., Nagar et al., 1999; Kukula et al., 1999), the resolution of the radio images is often insufficient to demonstrate the high degree of collimation seen in radio galaxies and radio-loud quasars.

Although compact starbursts may co-exist with AGNs in some Seyferts (e.g., Heckman et al., 1997; González-Delgado et al., 1998; Carilli et al., 1998), we have argued that the sub-pc scale, high brightness radio emission from T0109−383, NGC 2110, NGC 5252 and Mrk 926 is dominated by the central engine. Radio emission from a starburst region consists of synchrotron radiation from supernova remnants (SNR's) plus thermal free-free emission from HII regions. The brightness temperature of such a region cannot exceed $10^5$ K at $\nu >$ 1 GHz (Condon, 1992) and so the high brightnesses of our Seyfert nuclei, along with their sub-pc sizes rule out a starburst origin for the radio emission. In fact, these Seyfert nuclei show similar brightness temperatures to some radio-quiet quasars (Blundell & Beasley,

[3]An edge-on disk geometry is unlikely for Mrk 926, a Seyfert 1, and the inferred column density for this galaxy is much lower than that of NGC 2110 or NGC 5252. Thus the predicted radio flux from Mrk 926 will be lower than from NGC 2110 or NGC 5252.

1998) and LINERs (Falcke et al., 1999), which are also argued to be non-thermal emission from black-hole powered central engines rather than compact starbursts. In NGC 4388, the well-collimated radio jet also suggests the presence of an AGN, despite the lack of an unresolved, high brightness nucleus.

We can also rule out individual or a collection of extremely bright radio supernovae (RSN) as an explanation for the Seyfert core emission. Although these rare, bright RSN, of the kind observed in NGC 891 (van Gorkom et al. 1986), designated SN1986J and classified as an unusual type II radio supernova (Weiler, Panagia & Sramek, 1990), can display high brightness temperatures at the peak of their light curves (e.g. $10^9$ K at $\lambda$6 cm at the peak of the SN1986J light curve), their fluxes increase and decrease over a timescale of a few years. The $\lambda$6-cm flux of SN1986J doubled in approximately three years and halved again over the following three years. Measured VLA fluxes for our Seyfert cores have typically varied by less than 30% over $\sim$10 years and are therefore inconsistent with an RSN interpretation. In addition, the *maximum* inferred 8.4-GHz luminosity for SN1986J of $\sim 8 \times 10^{20}$ W Hz$^{-1}$ (calculated using the $\lambda$6-cm flux at the peak of the light curve, $\alpha^6_{3.6} = 0.7$, and assuming isotropic emission at a distance of 8.96 Mpc) is somewhat lower than the luminosities of our Seyfert nuclei (Table 2).

We therefore conclude that the high brightness temperatures ($> 10^8$ K), small sizes ($< 1$ pc) and absence of strong flux variations over $\sim$10-year timescales in T0109−383, NGC 2110, NGC 5252 and Mrk 926 are probably indicative of synchrotron self-absorption close to a jet-producing central engine. The lower limits to the brightness temperatures do not require relativistic motions, which is consistent with the non-relativistic proper motions observed in two Seyfert galaxies by Ulvestad et al., (1999).

### 5.4. Thermal Bremsstrahlung Emission in NGC 4388

Unlike the other four galaxies discussed in this paper, no high brightness temperature compact radio core is detected in NGC 4388 at 8.4 GHz. The observationally inferred brightness temperature of $2.4 \times 10^4$ K $< T_B < 2.2 \times 10^6$ K (the lower limit at 5 GHz, the upper limit at 8.4 GHz, see Section 4.3.1) is too low for synchrotron self absorption to be important. Instead we consider a model in which the emission is optically thin, thermal bremsstrahlung, compatible with the observed flat radio spectrum, from a gas with an electron temperature of $T_e$ (K).

Our bremsstrahlung model consists of a thermal plasma of uniform temperature, $T_e$, and density, $n_e$, that fills the emitting volume, $V$, with a filling factor $f$. The maximum

source volume is set by the MERLIN beamsize and assumes an ellipsoidal geometry (with semi-axes of 3.6 × 1.5 × 1.5 pc), while the minimum source size, as discussed in Section 4.3.1, is ∼0.3 pc, for which an edge-on disk geometry is assumed (disk diameter 0.4 pc, height 0.2 pc). Figures 4(a,b,c) show the allowed range of densities ($n_e$), opacities at 4.993 GHz ($\tau_{\rm ff}$) and ionized gas column densities ($N_e$) as a function of $T_e$, within the limits set by the possible source sizes.

As shown by the shaded area in Figure 4(b), the gas becomes optically thin at 4.993 GHz for $T_e > 10^{4.5}$ K, suggesting $n_e > 1.6 \times 10^4$ f $^{-0.5}$ cm$^{-3}$ for the MERLIN size limit, or $T_e > 10^{6.8}$ K and $n_e > 1.8 \times 10^6$ f $^{-0.5}$ cm$^{-3}$ for the smaller source size set by the VLBA limit. The larger electron density, for $f$=1, is intermediate between that expected in Seyfert narrow line regions (e.g., ∼$10^3$ cm$^{-3}$ - Koski, 1978) and broad line regions (∼$10^9$ cm$^{-3}$), consistent with the small size of the region, and similar to ionized gas densities of $10^5$–$10^7$ cm$^{-3}$ inferred from free-free absorption in the inner parsec of Mrk 231 and Mrk 348 (Ulvestad et al., 1999). Similarly high electron temperatures and densities have been derived for thermal emission from the torus gas in NGC 1068 (Gallimore et al., 1997), thus implying that we may be seeing the same phenomenon in NGC 4388.

The lower limit to the electron column density of $N_e > 7 \times 10^{22}$ cm$^{-2}$ (Figure 4c) is compatible with the total column of $4.2 \times 10^{23}$ cm$^{-2}$ inferred from the photoelectric absorption seen in the ASCA observed X-ray spectrum of NGC 4388 (Iwasawa et al., 1997). Demanding equality of ionized and total columns would imply $T_e > 10^6$ K.

If the radio emission is indeed thermal bremsstrahlung, we may calculate the predicted, intrinsic H$\beta$ flux from this gas using (e.g., Ulvestad, Wilson & Sramek, 1981):

$$F(H\beta)\ (\mathrm{erg\ cm^{-2}\ s^{-1}}) \ = \ 0.62\ T_e^{0.5}(K)\ g_{ff}^{-1}(\nu,\ Z,\ T)\ \alpha_{H\beta}^{eff}\ S_\nu(mJy),$$

where $S_\nu$ is the radio flux density, $\alpha_{H\beta}^{eff} = 3.01 \times 10^{-14}(T/10^4)^{-0.85}$ and $g_{ff}$ is the Gaunt factor. Taking $S_\nu$ = 2.1 mJy at 5 GHz, we predict $F(H\beta) < 4.0 \times 10^{-13}$ erg cm$^{-2}$ s$^{-1}$ for $T_e > 10^{4.5}$ K (Figure 4d). However the observed [OIII] flux of $1.86 \times 10^{-13}$ erg cm$^{-2}$ s$^{-1}$, through 1.″5×3″ (Corbin et al., 1988) or 2″×3.″5 apertures (Colina, 1992), and the [OIII] to H$\beta$ ratio of 11.2 (Phillips & Malin, 1982), result in a mean observed H$\beta$ flux of only $1.7 \times 10^{-14}$ erg cm$^{-2}$ s$^{-1}$ (which we treat as an upper limit to the H$\beta$ flux from the MERLIN source due to the large optical apertures compared to the radio sizes), a factor of 24 lower than our predicted value if $T_e = 10^{4.5}$ K. If our assumption of a thermal origin for the radio emission is correct, the difference between observed and predicted F(H$\beta$) suggests $A_V \gtrsim 3.0$ magnitudes of extinction towards the nucleus for $T_e$=$10^{4.5}$ K. Using the H$\beta$ flux measured by Dahari & De Robertis (1988) of $5.2 \times 10^{-14}$ erg cm$^{-2}$ s$^{-1}$ results in a lower extinction of $A_V \gtrsim 1.9$ mags. In addition, no broad Pa$\beta$, Br$\gamma$ or Br$\alpha$ lines are detected towards the nucleus (Blanco et al., 1990; Ruiz et al., 1994; Veilleux et al, 1997),

while a broad, off-nuclear H$\alpha$ line (Shields & Filippenko, 1988) is detected 4″ from the nucleus, consistent with scattered emission from the broad line region. A temperature in excess of $10^8$ K would be required to explain the low observed H$\beta$ flux in the absence of extinction and therefore, given the implication from optical studies that NGC 4388 harbors an obscured Seyfert type 1 nucleus, the moderately large value of extinction suggested by the radio data does not seem unreasonable.

Alternatively, not all of the radio emission might be thermal, and the base of a radio jet could provide a non-thermal contribution. However, any significant non-thermal contribution would be difficult to reconcile with the flat radio spectrum, given the low observed brightness temperature. We therefore favor the thermal emission model for the nuclear radio emission in NGC 4388.

## 6. Conclusions

We have used the VLBA at 8.4 GHz to study five Seyfert nuclei that contain flat spectrum radio sources, in order to determine whether the flat-spectrum nuclear radio emission, detected in VLA studies, represents thermal emission from the accretion disk/obscuring torus or synchrotron self-absorbed emission from a compact radio core source.

Four of the five sources were detected (T0109−383, NGC 2110, NGC 5252, Mrk 926) and show compact, unresolved cores with brightness temperatures, $T_B > 10^8$ K, total luminosities at 8.4 GHz of $\sim 10^{21}$ W Hz$^{-1}$ and sizes, on average, less than 1 pc. We conclude that the sub-pc scale radio emission in these sources is non-thermal and self absorbed and, hence, dominated by the central engine. In addition to the core emission, NGC 2110 shows extended emission which may represent the inner parts of the radio jets. However, we find no evidence of thermal disk-like emission, extended perpendicular to the collimation axis, in any of these sources to a 3-$\sigma$ limit of $\sim 10^6$ K.

The putative nucleus of NGC 4388 is not detected with the VLBA but is detected with MERLIN at 5 GHz. The observationally inferred brightness temperature of $2.4 \times 10^4$ K $< T_B < 2.2 \times 10^6$ K (the lower limit at 5 GHz, the upper limit at 8.4 GHz) is too low for synchrotron self absorption to be important. Instead we have proposed a model in which the emission is optically thin, free-free thermal bremsstrahlung emission from a gas with an electron temperature of $T_e > 10^{4.5}$ K and density $n_e > 1.6 \times 10^4$ f $^{-0.5}$ cm$^{-3}$ (where f is the volume filling factor). The larger inferred values of $T_e > 10^{6.8}$ K and $n_e > 1.8 \times 10^6$ f $^{-0.5}$ cm$^{-3}$ for the smaller source size set by the VLBA limit, are similar

to the values of $\sim 10^{6.8}$ K and $\sim 10^{6.8}$ cm$^{-3}$ found for thermal emission from the torus gas in NGC 1068 (Gallimore et al., 1997), thus implying that we may be seeing the same phenomenon in NGC 4388. Sensitive VLBA observations of NGC 4388 at 1.4 GHz or 2.3 GHz are required to spatially resolve the emitting region and determine its exact physical properties.

We thank Pierre Ferruit, Neil Nagar and Dave Shone for useful discussions, and Peter Thomasson for help with the MERLIN data. The National Radio Astronomy Observatory is a facility of the National Science Foundation operated under cooperative agreement by Associated Universities, Inc. MERLIN is a U.K. national facility operated by the University of Manchester on behalf of PPARC. This research has made use of: the United States Naval Observatory (USNO) Radio Reference Frame Image Database (RRFID), NASA's Astrophysics Data System Abstract Service (ADS) and the NASA/IPAC Extragalactic Database (NED), which is operated by the Jet Propulsion Laboratory, California Institute of Technology, under contract with the National Aeronautics and Space Administration. This research was supported by the National Science Foundation under grant AST 9527289 and NASA under grant NAG 81027.

## REFERENCES

Acosta-Pulido, J.A., Vila-Vilaró, B., Pérez-Fournon, I., Wilson, A.S. & Tsvetanov, Z.I., 1996, ApJ, 464, 177

Alonso-Herrero, A., Ward, M.J. & Kotilainen, J., 1996, Vistas in Astronomy, 40, 221

Antonucci, R.R.J., 1993, ARA&A, 31, 473

Antonucci, R.R.J. & Miller, J.S., 1985, ApJ, 297, 621

Antonucci, R..R.J. & Ulvestad, J.S., 1985, ApJ, 294, 158

Baars, J.W.M., Genzel, R., Pauliny-Toth, I.I.K. & Witzel, A., 1977, A&A, 61, 99

Balsara, D.S. & Krolik, J.H., 1993, ApJ, 401, 109

Baker, A.J. & Scoville, N.Z., 1998, BAAS, 192, 3605

Bassani, L., Dadina, M., Maiolino, R., Salvati, M., Risaliti, G., Della Ceca, R., Matt, G. & Zamorani, G., 1999, ApJS, 121, 473

Beasley, A.J. & Conway, J.E., 1995, in ASP Conf. Series 82, Very Long Baseline Interferometry and the VLBA, eds. J.A. Zensus, P.J. Diamond & P.J. Napier (San Francisco: ASP), 327

Bicknell, G.V., Dopita, M.A., Tsvetanov, Z.I. & Sutherland, R.S., 1998, ApJ, 495, 680

Blanco, P. R., Ward, M. J., & Wright, G. S. 1990, MNRAS, 242, 4P

Blandford, R.D. & Begelman, M.C, 1998, MNRAS, 303, L1

Blundell, K.M. & Beasley, A.J., 1998, MNRAS, 299, 165

Boisson, C. & Durret, F., 1986, A&A, 168, 32

Bradt, H.V., Burke, B.F., Canizares, C.R., Greenfield, P.E., Kelley, R.L., McClintock, J.E., Koski, A.T. & Van Paradijs, J., 1978, ApJ, 226, L111

Briggs, D.S., 1995, Ph.D. Thesis, N.M. Institute of Mining & Technology

Browne, I.W.A., Wilkinson, P.N., Patnaik, A.R. & Wrobel, J.M., 1998, MNRAS, 293, 257

Carral, P., Turner, J. L., & Ho, P. T. P. 1990, ApJ, 362, 434

Carilli, C.L., Wrobel, J.M. & Ulvestad, J.S., 1998, AJ, 115, 928

Carollo, C.M., Franx, M., Illingworth, G.D. & Forbes, D.A., 1997, ApJ, 481, 710

Clements, E.D., 1981, MNRAS, 197, 829

Clements, E.D., 1983, MNRAS 204, 811

Colina, L., 1992, ApJ, 386, 59

Condon, J.J., Huang, Z.-P., Yin, Q.F. & Thuan, T.X., 1991, ApJ, 378, 65

Condon, J.J., 1992, in "Testing the AGN Paradigm", AIP Conference Proceedings 254, eds. Holt, S.S., Neff, S.G., Urry, C.M., 629

Corbin, M.R., Baldwin, J.A. & Wilson, A.S., 1988, ApJ, 334, 584

Crusius-Waetzel, A.R. & Lesch, H., 1998, A&A, 338, 399

Dahari, O. & De Robertis M.M., 1988, ApJS, 67, 249

de Bruyn, A.G. & Wilson, A.S., 1978, A&A, 64, 433

de Vaucouleurs, G., de Vaucouleurs, A., Corwin, H.G., Jr., Buta, R.J., Paturel, G. & Fouqué, P., 1991, Third Reference Catalogue of Bright Galaxies (Springer, Berlin)

Downes, D. & Solomon, P.M., 1998, ApJ, 507, 615

Falcke, H., Ho, L.C., Ulvestad, J.S., Wilson, A.S. & Nagar, N.M., 1999, in Proceedings of the "International Symposium on Astrophysics Research And Science Education at The Vatican Observatory", ed. C. Impey, in press

Falcke, H., Wilson, A.S. & Simpson, C., 1998, ApJ, 502, 199

Fey, A. L. & Charlot, P. 1997, ApJS, 111, 95

Fernandes, R.C., Jr. & Terlevich, R., 1995, MNRAS, 272, 423

Ford, H.C., et al., 1994, ApJ, 435, L27

Fosbury, R.A.E. & Sansom, A.E., 1983, MNRAS, 204, 1231

Gallimore, J.F., Baum, S.A. & O'Dea, C.P., 1997, Nature, 388, 852

George, I.M., Turner, T.J., Netzer, H, Nandra, K., Mushotzky, R.F. & Yaqoob, T., 1998, ApJS, 114, 73

González-Delgado, R.M., Heckman, T., Leitherer, C., Meurer, G., Krolik, J., Wilson, A.S., Kinney, A. & Koratkar, A., 1998, ApJ, 505, 174

Greisen E.W. & Murphy, P.P., 1998, The AIPS Cookbook, chapter 9, online at [http://www.cv.nrao.edu/aips/cook.html]

Greenhill, L.J., Jiang, D.R., Moran, J.M., Reid, M.J., Lo, K.Y. & Claussen, M.J., 1995, ApJ, 440, 619

Haehnelt, M.G. & Rees, M.J., 1993, MNRAS, 263, 168

Heckman, T.M., González-Delgado, R., Leitherer, C., Meurer, G.R., Krolik, J., Wilson, A.S., Koratkar, A. & Kinney, A., 1997, ApJ, 482, 114

Herrnstein, J.R., Greenhill, L.J. & Moran, J.M., 1996, ApJ, 468, L17

Hough, D.H. et al., 1999, ApJ, 511, 84

Hummel, E. & Saikia, D.J., 1991, A&A, 249, 43

Iwasawa, K., Fabian, A.C., Ueno, S., Awaki, H., Fukazawa, Y., Matsushita, K. & Makishima, K., 1997, MNRAS, 285, 683

Jaffe, W., Ford, H.C., Ferrarese, L., van den Bosch, F & O'Connell, R.W., 1993, Nature, 364, 213

Kato, S., Fukue, J. & Mineshige, S., 1998, "Black-hole accretion disks", eds. S. Kato, J. Fukue, and S. Mineshige; Publisher: Kyoto, Japan: Kyoto University Press, 1998

Kedziora-Chudczer, L., Jauncey, D.L., Wieringa, M.H., Walker, M.A., Nicolson, G.D., Reynolds, J.E., Tzioumis, A.K., 1997, ApJ 490, L9

Kellermann, K.I. & Pauliny-Toth, I.I.K., 1969, ApJ, 155, L71

Kellermann, K.I. & Pauliny-Toth, I.I.K., 1981, ARA&A, 19, 373

Kellermann, K.I., Vermeulen, R.C., Zensus, J.A. & Cohen, M.H, 1998, AJ, 115, 1295

Koski, A.T., 1978, ApJ, 223, 56

Krolik, J.H. & Begelman, M.C., 1988, ApJ, 329, 702

Krolik, J.H. & Lepp, S., 1989, 347, 179

Kukula, M.J., Ghosh, T., Pedlar, A., Schilizzi, R.T., Miley, G.K., De Bruyn, A.G. & Saikia, D.J., 1993, MNRAS, 264, 893

Kukula, M.J., Pedlar, A., Baum, S.A. & O'Dea, C.P., 1995, MNRAS, 276, 1262

Kukula, M.J., Ghosh, T., Pedlar, A. & Schilizzi, R.T, 1999, ApJ, in press

Lähteenmäki, A., Valtaoja, E. & Wiik, K., 1999, ApJ, 511, 112

Ma, C. et al., 1998, AJ, 116, 516

Malaguti, G. et al., 1999, A&A, 342, L41

Maloney, P.R., Begelman, M.C. & Pringle, J.E., 1996, ApJ, 472, 582

Matt, G. et al., 1997, A&A, 325, L13

Miyoshi, M., Moran., J., Herrnstein, J., Greenhill, L., Nakai, N., Diamond, P. & Inoue, M., 1995, Nature, 373,127

Morganti, R., Tsvetanov, Z.I., Gallimore, J. & Allen, M.G., 1999, A&AS, in press

Morse, J.A., Cecil, G., Wilson, A.S. & Tsvetanov, Z.I., 1998, ApJ, 505, 159

Mundell, C.G., Pedlar, A., Baum, S.A., O'Dea, C.P., Gallimore, J.F. & Brinks, E., 1995, MNRAS, 272, 355

Murayama, T., Taniguchi, Y., Iwasawa, K., 1998, AJ, 115, 460

Nagar, N.M., Wilson, A.S., Mulchaey, J.S. & Gallimore, J.F., 1999, ApJS, 120, 209

Napier, P.J., Bagri, D.S., Clark, B.G., Rogers, A.E.E., Romney, J.D., Thompson, A.R. & Walker, R.C., 1994, Proc IEEE, 82, 658

Narayan, R. & Yi, I., 1994, ApJ, 428, L13

Pearson, T.J. et al., 1998, in ASP Conference Series 144, Radio Emission from Galactic and Extragalactic Compact Sources, eds. J.A. Zensus, G.B. Taylor, & J.M. Wrobel (San Francisco: ASP), 17

Peck, A.B. & Beasley, A.J., 1998, in ASP Conf. Series 144, Radio Emission from Galactic and Extragalactic Compact Sources, eds. J.A. Zensus, G.B. Taylor, & J.M. Wrobel (San Francisco: ASP), 155

Peck, A.B. & Taylor, G.B., 1998, ApJ, 502, L23

Penston, M.V., Fosbury, R.A.E., Boksenberg, A., Ward, M.J. & Wilson, A.S., 1984, MNRAS, 208, 347

Peterson, B.M., 1997, An Introduction to Active Galactic Nuclei, (Cambridge: Cambridge University Press)

Phillips, M.M. & Malin, D.F., 1982, MNRAS, 199, 905

Pier, E.A. & Krolik, J.H., 1992, ApJ, 399, L23

Pier, E.A. & Voit, G.M., 1995 ApJ, 450, 628

Pogge, R.W., 1988, ApJ, 332, 702

Prieto, M.A. & Freudling, W., 1993, ApJ, 418, 668

Prieto, M.A. & Freudling, W., 1996, MNRAS, 279, 63

Pringle, J.E., 1996, MNRAS, 281, 357

Readhead, A.C.S., 1994, ApJ, 426, 51

Richstone, D. et al., 1998, Nature, 395, 14

Roy, A.L., Colbert, E.J.M., Wilson, A. S., Ulvestad, J.S., 1998, ApJ, 504, 147

Roy, A.L., Norris, R.P., Kesteven, M.J., Troup, E.R. & Reynolds, J.E., 1994, ApJ, 432, 496

Ruiz, M., Rieke, G. H., & Schmidt, G. D. 1994, ApJ, 423, 608

Sadler, E.M., Slee, O.B., Reynolds, J.E. & Roy, A.L., 1995, MNRAS, 276, 1373

Shields, J.C. & Filippenko, A.V., 1988, ApJ, 332, L55

Silk, J. & Rees, M.J., 1998, A&A, 331, L1

Smith, M.G., 1975, ApJ, 202, 591

Stone, J.L., Jr., Wilson, A.S. & Ward, M.J., 1988, ApJ, 330, 105

Tadhunter, C. & Tsvetanov, Z.I., 1989, Nature, 341, 422

Taylor, G.B., O'Dea, C.P., Peck, A.B. & Koekemoer, A.M., 1999, ApJ, 512, L27

Tran, H.D., 1995, ApJ, 440, 578

Turner, T.J., George, I.M., Nandra, K. & Mushotzky, R.F., 1997, ApJS, 113, 23

Ulvestad, J. S., Gurvits, L. I., & Linfield, R. P. 1997, in High Sensitivity Radio Astronomy, ed N. Jackson & R. Davis (Cambridge: Cambridge University Press), 252

Ulvestad, J. S., & Linfield, R. P. 1998, in ASP Conf. Series 144, Radio Emission from Galactic and Extragalactic Compact Sources, ed. J. A. Zensus, G. B. Taylor, & J. M. Wrobel (San Francisco: ASP), 397

Ulvestad, J.S., Roy, A.L., Colbert, E.J.M. & Wilson, A.S., 1998, ApJ, 496, 196

Ulvestad, J.S., Wilson, A.S. & Sramek, 1981, ApJ, 247, 419

Ulvestad, J.S. & Wilson, A.S., 1983, ApJ 264, L7

Ulvestad, J.S. & Wilson, A.S., 1984a, ApJ, 278, 544

Ulvestad, J.S. & Wilson, A.S., 1984b, ApJ, 285, 439

Ulvestad, J.S. & Wilson, A.S., 1989, ApJ, 343, 659

Ulvestad, J.S., Wrobel, J.M., Roy, A.L., Wilson, A.S., Falcke, H. & Krichbaum, T.P., 1999, ApJ, 517, L81

Ulvestad, J.S., Wrobel, J.M. & Carilli, C.L., 1999, ApJ, 516, 134

van der Marel, R.P., 1999, AJ, 117, 744

van Gorkom, J., Rupen, M., Knapp, G., Gunn, J, Neugebauer, G. & Matthews, K., 1986, IAUC, 4248, 1

van Moorsel, G., Kemball, A., & Greisen, E., 1996, in ASP Conf. Series 101, Astronomical Data Analysis Software and Systems V, eds., G.H. Jacoby & J. Barnes (San Francisco: ASP), 37

Veilleux, S., 1991, ApJ, 369, 331

Veilleux, S., Bland-Hawthorn, J., Cecil, G., Tully, R.B. & Miller, S.T, 1999, ApJ, 520,

Veilleux, S., Goodrich, R.W. & Hill, G.J., 1997, ApJ, 477, 631

Walker, R.C., 1995, in ASP Conf. Series 82, Very Long Baseline Interferometry and the VLBA, eds. J.A. Zensus, P.J. Diamond & P.J. Napier (San Francisco: ASP), 247

Ward, M.J., Wilson, A.S., Penston, M.V., Elvis, M., Maccacaro, T. & Tritton, K.P., 1978, ApJ, 223, 788

Weaver, K.A., Mushotzky, R.F., Serlemitsos, P.J., Wilson, A.S., Elvis, M. & Briel, U., 1995a, ApJ, 442, 597

Weaver, K.A., Nousek, J., Yaqoob, T., Hayashida, K. & Murakami, S., 1995b, ApJ, 451, 147

Weiler, K.W., Panagia, N. & Sramek, R.A., 1990, ApJ, 364, 611

Wilson, A.S., Baldwin, J.A. & Ulvestad, J.S., 1985, ApJ, 291, 627

Wilson, A.S. & Meurs, E.J.A., 1982, A&AS, 50 217

Wilson, A.S. & Raymond, J.C., 1999, ApJ, 513, 115

Wilson, A.S. et al., 1998, ApJ, 505, 587

Wilson, A.S. & Tsvetanov, Z.I., 1994, AJ, 107, 1227

Wilson, A.S. & Ulvestad, J.S., 1983, ApJ, 275, 8

Wrobel, J.M., Patnaik, A.R., Browne, I.W.A & Wilkinson, P.N., 1998, BAAS, 30, 1308

Fig. 1.— Radio continuum images of the sources detected at 8.4 GHz with the VLBA - T0109−383, NGC 2110, NGC 5252 and Mrk 926. The 8.4-GHz VLBA images are shown in the right hand panels, with the restoring FWHM beamsize shown as an ellipse in the bottom left corner of each image and linear scale marked in the bottom right corner. A VLA image of the larger scale structure of each source is shown in the corresponding left hand panel (from Nagar et al. (1999) for NGC 2110 and NGC 5252, and from unpublished observations by J.A. Braatz, L.L. Dressel & A.S. Wilson for T0109−383 and Mrk 926). Contour levels for the VLBA images and unpublished VLA images are given in Table 5.

Fig. 2.— MERLIN 5-GHz radio continuum image of NGC 4388. The nucleus is marked M1 and the secondary weak feature (possibly a component in the radio jet) is marked M2. The beamsize is indicated by an ellipse in the lower left corner. The contour levels, in multiples of 3×r.m.s., are (–2, –1, 1, 2, 3, 4) × 0.3 mJy beam$^{-1}$ or $T_B$ = (–2, –1, 1, 2, 3, 4) × 5.9×10$^3$ K (beamsize 91.0 × 39.5 mas).

Fig. 3.— (a) VLA 8.4-GHz radio continuum image (full resolution image produced from data presented by Falcke et al., 1998) of the 1$''$.9 central double source in NGC 4388 (each component is marked V1 and V2, with V1 taken to be the core); (b) Super-resolved VLA image, from the same $(u, v)$ data as used for (a), revealing collimated ejection from the core and bending of the jet at V2. The crosses indicate the two MERLIN components (M1 and M2), where M1 is coincident with the core and M2 coincides with a protrusion in the 8.4-GHz VLA contours in the direction of the jet. The contour levels for both images are (–1, 1, 2, 4, 8, 16, 32) × 90 $\mu$Jy beam$^{-1}$ and the beamsizes (shown in the lower left corner of each image) are (a) 0$''$.70 × 0$''$.22 and (b) 0$''$.22 × 0$''$.22.

Fig. 4.— Range of possible values of (a) electron density, $n_e$, (b) free-free opacity at 4.993 GHz, $\tau_{\rm ff}$, (c) column density of ionized gas, $N_e$, and (d) predicted $H_\beta$ flux, assuming the radio emission from NGC 4388, at 4.993 GHz, is free-free thermal bremsstrahlung emission from an ionized gas with an electron temperature, $T_e$. Upper and lower limits to the plotted quantities are derived from the lower and upper limits to the source size (Section 4.3.1); we assumed the maximum source volume (MERLIN limit) corresponds to an ellipsoid (with semi-axes 3.6 × 1.5 × 1.5 pc), and the minimum volume (VLBA limit) corresponds to an edge-on disk (with diameter, 0.4 pc, and height, 0.2 pc). The permitted values for an optically thin plasma (as indicated by the flat radio spectrum) are indicated by the shading.

Table 1: Observing parameters for the 8.4-GHz VLBA observations of Seyfert galaxies and calibrators. Measured positions, derived from Gaussian fitting, for the check sources are also given. The surveys from which the positions of the phase calibrators were selected are listed below as footnotes, along with the corresponding positional accuracy.

| Target Seyfert | T0109−383 | NGC 2110 | NGC 4388 | NGC 5252 | Mkn 926 |
|---|---|---|---|---|---|
| Date of observations | 07 Aug 1997 | 9 Aug 1997 | 12 Jun 1998 | 14 Jun 1998 | 21 Jul 1997 |
| Phase calibrator | J0106−4034[a] | J0541−0541[b] | J1207+1211[c] | J1320+0140[d] | J2255−0844[a] |
| Position used (J2000) | 01h06m45.1080s | 05h41m38.0834s | 12h07m12.625s | 13h20m26.7938s | 22h55m04.2398s |
| | −40°34′19.″960 | −05°41′49.″428 | 12°11′45.″89 | 01°40′36.″786 | −08°44′04.″022 |
| Source + phase cali- | | | | | |
| -brator cycle time | ∼2 + 1 min | ∼4 + 1 min | ∼3 + 1 min | ∼3 + 1 min | ∼4 + 1 min |
| 'Check' calibrator | J0044−3530 | J0607−0834 | J1214+0829 | J1359+0159 | J2246−1206 |
| Position used (J2000) | 00h44m41.229s | 06h07m59.699s | 12h14m59.914s | 13h59m27.1478s | 22h46m18.232s |
| | −35°30′41.″63 | −08°34′49.″98 | 08° 29′ 22.″53 | 01° 59′ 54.″543 | −12°06′51.″28 |
| Position measured | — | 06h07m59.6975s | 12h14m59.913s | 13h59m27.1512s | 22h46m18.2313s |
| | | −08°34′49.″994 | 08°29′22.″56 | 01°59′54.″531 | −12°06′51.″262 |
| Times on 'check' cal. | 3 × 1 min | 4 × 1 min | 12 × 1 min | 13 × 1 min | 4 × 1 min |
| Online fringe-finder | 3C454.3 | DA193 | 3C273 | 3C273 | 3C454.3 |
| Total time on source | ∼2.5 hrs | ∼3.2 hrs | ∼6.0 hrs | ∼5.8 hrs | ∼3.3 hrs |

[a,b]Ma et al., 1998 (2.5, 0.4 mas) [c]Browne et al., 1998;Wrobel et al., 1998 (14 mas) [d]Peck & Beasley, 1998 (<5 mas)

Table 2: Results of VLBA observations. Galaxy names, positions, peak and integrated fluxes from single component Gaussian fitting, and beamsizes ($\theta$) are listed (columns 1–5). Lower limits to the brightness temperatures ($T_B$ (K), column 6) are derived from the given peak flux, assuming an upper limit to the source size of half of the beamsize; for NGC 2110, the peak flux of the unresolved component (given in Table 3) is used instead. The luminosity at 8.4 GHz (L, column 7) is calculated using the total flux density and assuming isotropic emission at the distance of the galaxy (D, column 8; obtained assuming $H_0 = 75$ km s$^{-1}$ Mpc$^{-1}$ and $q_0 = 0.5$).

| Seyfert | Fitted position (J2000.0)(R.A.) (J2000.0)(Dec.) | 8.4-GHz Peak Flux (mJy beam$^{-1}$) | 8.4-GHz Total Flux (mJy) | $\theta$ (mas) (*pc*) | $T_B$ (K) ($\times 10^8$ K) | L ($\times 10^{21}$) (W Hz$^{-1}$) | D (Mpc) |
|---|---|---|---|---|---|---|---|
| T0109−383 | 01 11 27.6413 | 9.9 ±0.6 | 11.0± 0.7 | 1.96 × 0.63 | >8.1 | 2.7 | 46.6 |
| | −38 05 00.477 | | | *0.45 × 0.14* | | | |
| NGC 2110[a] | 05 52 11.3762 | 16.6 ± 0.8 | 29.5±1.5 | 1.88 × 0.72 | >6.0 | 3.1 | 30.4 |
| | −07 27 22.513 | | | *0.28 × 0.11* | | | |
| NGC 5252 | 13 38 15.8698 | 7.9 ±0.4 | 9.1± 0.5 | 2.01 × 0.95 | >4.2 | 8.8 | 92.4 |
| | +04 32 33.513 | | | *0.91 × 0.43* | | | |
| Mkn 926 | 23 04 43.4776 | 4.6 ±0.2 | 5.0± 0.3 | 2.82 × 1.02 | >1.7 | 2.1 | 191.4 |
| | −08 41 08.629 | | | *2.64 × 0.95* | | | |

[a]See Table 3 for properties of multiple components present in NGC 2110.

Table 3: Results of Gaussian fitting to the emission from NGC 2110; three components are detected, which are identified (column 1) as an unresolved 'core', north-south 'jet' emission and a northern 'knot'. The positions of each component (column 5) relative to the core position (column 2) are given with positive offsets north of the core. Peak and integrated fluxes are given in columns 3 & 4, along with deconvolved sizes and position angles (column 6, 7) for the marginally resolved components.

| Component | Fitted position (J2000.0)(R.A.) (J2000.0)(Dec.) | 8.4 GHz Peak Flux (mJy beam$^{-1}$) | 8.4-GHz Total Flux (mJy) | Offset of fitted component centroid, $\Delta$mas relative to 'core' | Deconvolved size (mas) | PA (deg) |
|---|---|---|---|---|---|---|
| Unresolved 'core' | 05 52 11.3762 –07 27 22.513 | 8.0 ± 0.5 | 7.5 ±0.4 | 0 | 0 | 0 |
| N-S 'jet' | - | 8.7±0.5 | 13.1 ± 0.7 | +0.21 | 1.41 × 0.36 (±0.3) (±0.3) | 8.5 (±0.8) |
| Northern 'knot' | - | 5.0 ± 0.3 | 6.0 ± 0.3 | +1.95 | 0.75 × 0.12 (±0.4) (±0.12) | 137 (±90) |

Table 4: Upper table (a) shows the results of Gaussian fitting to the 5-GHz core emission in NGC4388, imaged with MERLIN. Fitted position, peak brightness, integrated flux density and beam size are given. The lower table (b) shows the corresponding derived brightness temperature $T_B$(K) (calculated using the measured MERLIN peak brightness and beamsize) and the *predicted* VLBA brightness temperatures at 8.4 GHz, assuming the spectral indices given, the VLBA beamsize given and that the source is unresolved with the VLBA. These predicted VLBA brightness temperatures exceed the observed value, allowing a lower limit to the source size to be determined (Section 4.3.1).

**(a) Results of Gaussian fitting to 5 GHz MERLIN image of NGC4388.**

| Seyfert | Fitted position (B1950.0)(R.A.) (B1950.0)(Dec.) | 5-GHz Peak Flux (mJy/beam) | 5-GHz Integrated Flux (mJy) | MERLIN Beamsize (mas) |
|---|---|---|---|---|
| NGC4388 | 12 23 14.646 12 56 20.20 | 1.2±0.1 | 2.1±0.3 | 91.0 × 39.5 |

**(b) Derived MERLIN 5-GHz and predicted VLBA 8.4-GHz brightness temperatures.**

| Derived $T_B$ ($10^4$ K) (at 5 GHz) | VLBA Beamsize | Assumed $\alpha$ from $\nu$=5 to 8.4 GHz | *Predicted* $T_B$ ($10^6$ K) (at 8.4 GHz) |
|---|---|---|---|
| >2.4 | 2.52×1.46 mas | 0 | 8.3 |
| | (0.23×0.14 pc) | 0.26 | 7.3 |

Table 5: Upper table lists contour levels (column 2), plotted as multiples of 3 × r.m.s in the image (column 3), and beamsizes (column 4) for the VLBA images in Figure 1. Brightnesses (mJy beam$^{-1}$) are converted to $T_B$ ($10^6$ K) using the corresponding VLBA beamsizes. Lower table lists contour levels (column 2) for the unpublished VLA images of T0109−383 and Mrk 926 shown in Figure 1, plotted as multiples of 3 × r.m.s in the image (column 3). The VLA beamsizes are given in column 4.

| Seyfert | 8.4-GHz VLBA Contour Levels (multiples of 3 × r.m.s.) | 3 × r.m.s. (mJy beam$^{-1}$) | ($10^6$ K) | Beamsize (mas) |
|---|---|---|---|---|
| T0109−383 | –1, 1, 2, 4, 8, 16 | 0.45 | 9.2 | 1.96 × 0.63 |
| NGC 2110 | –1, 1, 2, 4, 8, 16, 32 | 0.28 | 5.3 | 1.88 × 0.72 |
| NGC 5252 | –1, 1, 2, 4, 8, 16 | 0.30 | 4.0 | 2.01 × 0.95 |
| Mkn 926 | –1, 1, 2, 4, 8, 16 | 0.14 | 1.2 | 2.82 × 1.02 |
| | 8.4-GHz VLA Contour Levels (multiples of 3 × r.m.s.) | 3 × r.m.s. (mJy beam$^{-1}$) | | Beamsize ($''$) |
| T0109−383 | –1, 1, 2, 4, 8, 16, 32, 64 | 0.11 | | 0.41 × 0.17 |
| Mkn 926 | –1, 1, 2, 4, 8, 16, 32 | 0.12 | | 0.27 × 0.21 |

**Figure 1**

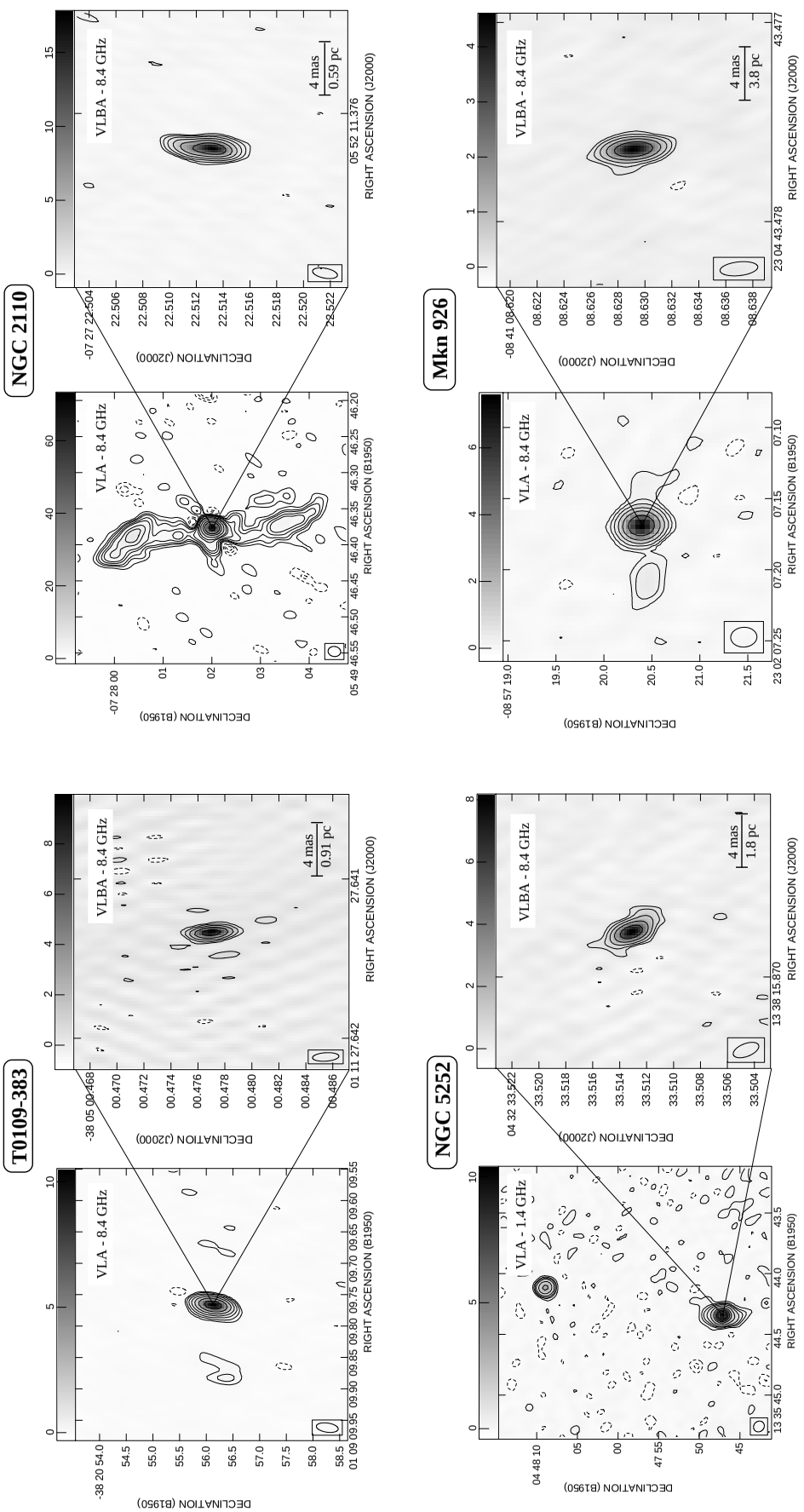
NGC 2110
VLA - 8.4 GHz
VLBA - 8.4 GHz
4 mas
0.59 pc
DECLINATION (B1950)
DECLINATION (J2000)
RIGHT ASCENSION (B1950)
RIGHT ASCENSION (J2000)
Mkn 926
VLA - 8.4 GHz
VLBA - 8.4 GHz
4 mas
3.8 pc
T0109-383
VLA - 8.4 GHz
VLBA - 8.4 GHz
4 mas
0.91 pc
NGC 5252
VLA - 1.4 GHz
VLBA - 8.4 GHz
4 mas
1.8 pc

**Figure 2**

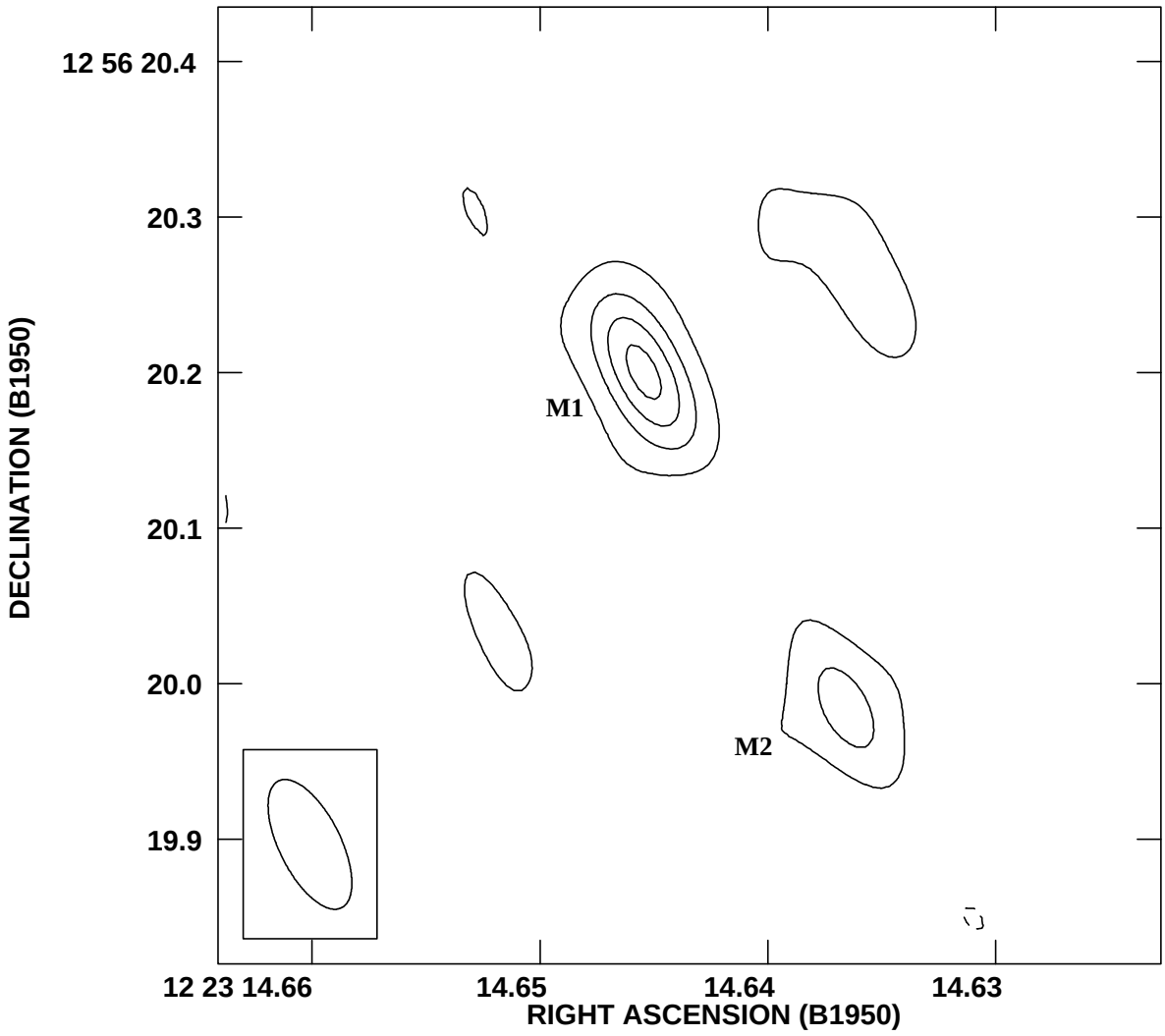
12 56 20.4
20.3
20.2
20.1
20.0
19.9
DECLINATION (B1950)
M1
M2
12 23 14.66
14.65
14.64
14.63
RIGHT ASCENSION (B1950)

**Figure 3**

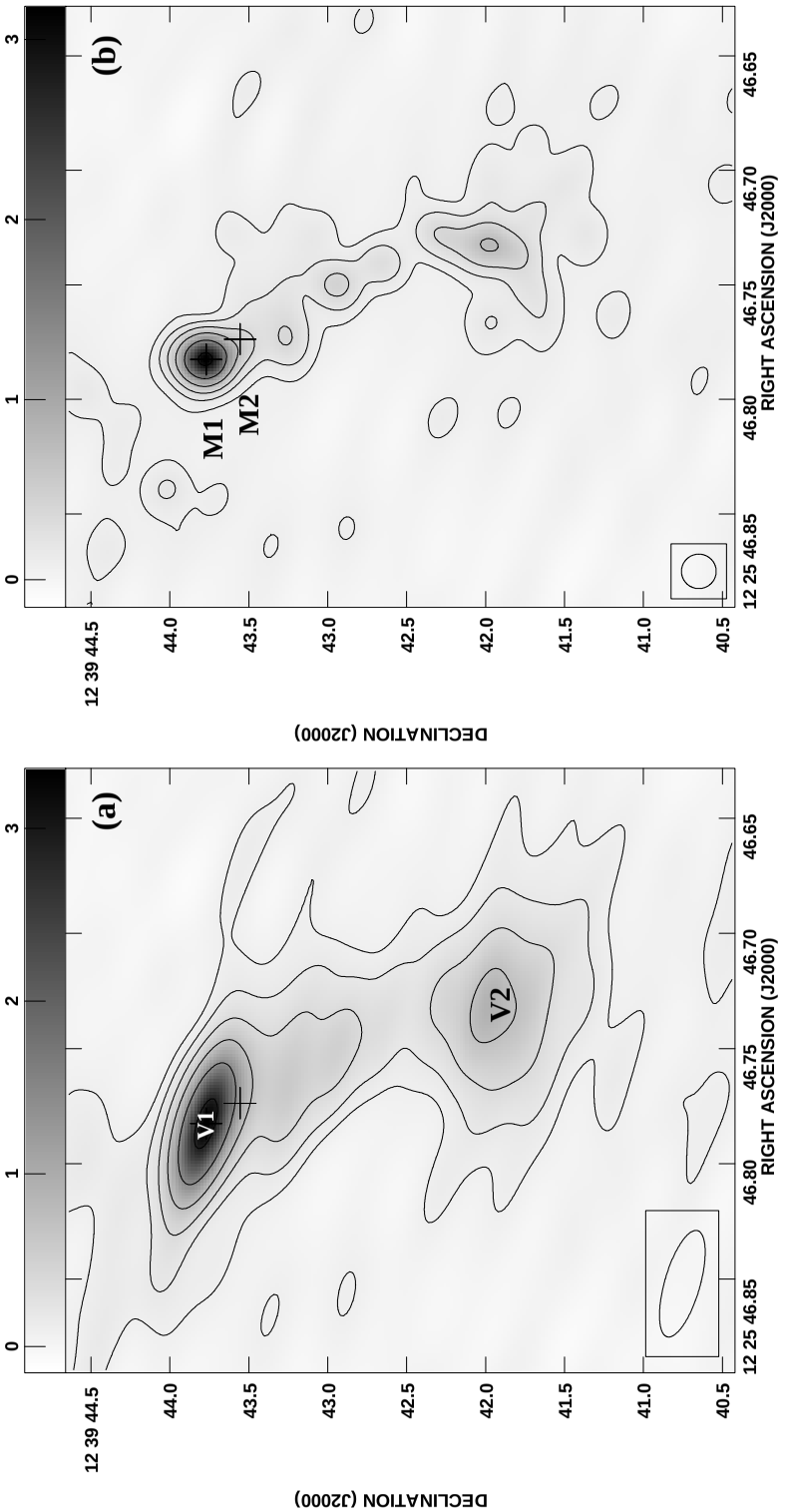
(b)
M1
M2
(a)
V1
V2
DECLINATION (J2000)
RIGHT ASCENSION (J2000)
12 39 44.5
44.0
43.5
43.0
42.5
42.0
41.5
41.0
40.5
12 25 46.85
46.80
46.75
46.70
46.65
0
1
2
3

**Figure 4**

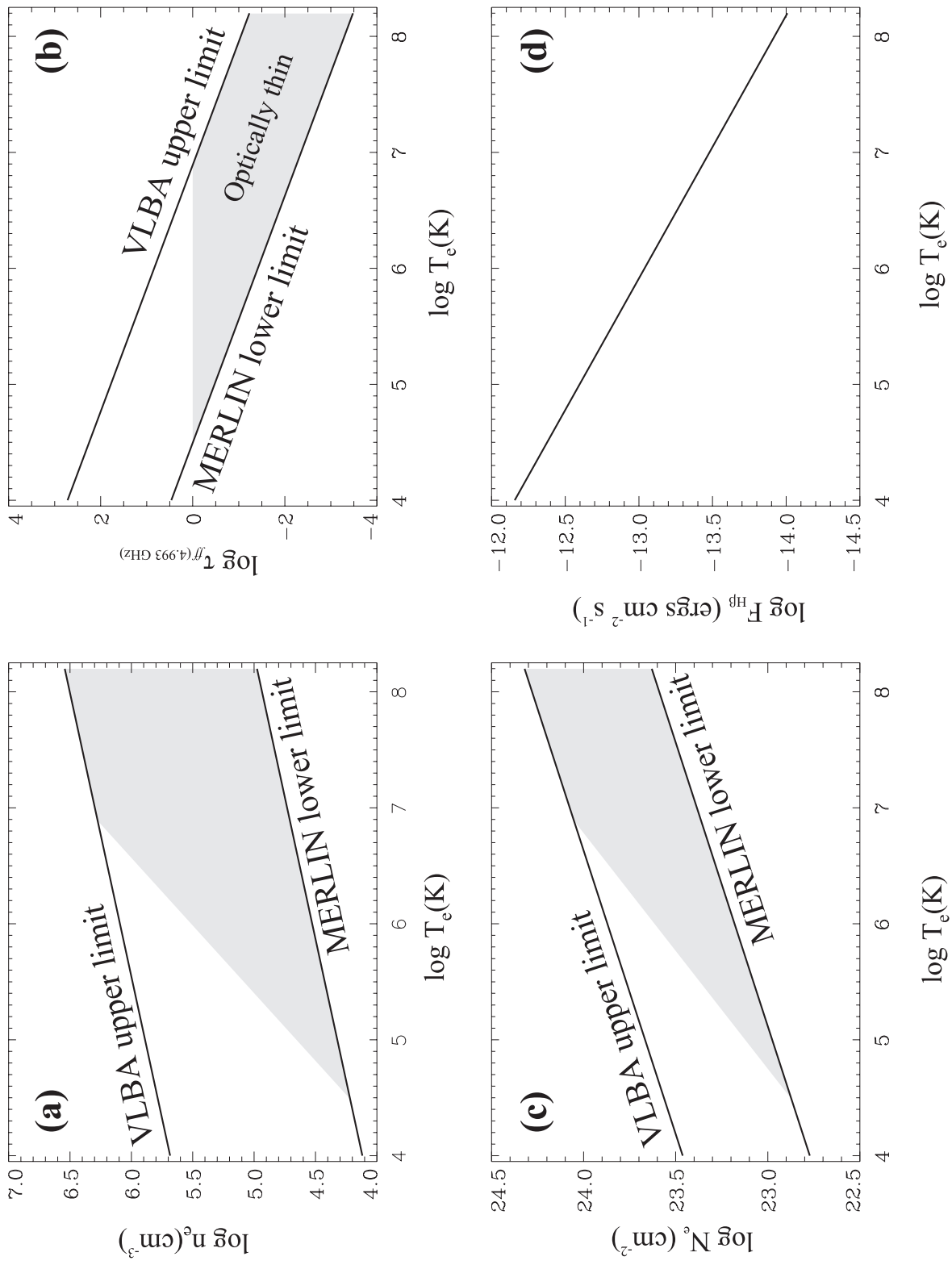
(a)
VLBA upper limit
MERLIN lower limit
log n$_e$(cm$^{-3}$)
log T$_e$(K)
(b)
VLBA upper limit
Optically thin
MERLIN lower limit
log τ$_{ff}$(4.993 GHz)
log T$_e$(K)
(c)
VLBA upper limit
MERLIN lower limit
log N$_e$ (cm$^{-2}$)
log T$_e$(K)
(d)
log F$_{H\beta}$ (ergs cm$^{-2}$ s$^{-1}$)
log T$_e$(K)